Available online at www.sciencedirect.com

jmr&t Journal of Materials Research and Technology

www.jmrt.com.br

Original Article

Implications of carbon, nitrogen and porosity on the $\gamma \rightarrow \alpha'$ martensite phase transformation and resulting hardness in PM-steel Astaloy 85Mo

James Damon, Stefan Dietrich, Volker Schulze*

Institute for Applied Materials (IAM-WK), Karlsruhe Institute of Technology (KIT), Karlsruhe, Germany

ARTICLE INFO

Article history:
Received 20 January 2020
Accepted 9 May 2020
Available online 10 June 2020

Keywords:
PM steels
Dilatometry
Martensitic transformation
Carbon nitrogen effects
Porosity dependence

ABSTRACT

This study aims at a thorough characterization of the relationship of interstitially solved carbon and nitrogen on the $\gamma \rightarrow \alpha'$ transformation in PM steels, the accompanied volume change and the resulting hardness. Furthermore, the investigations include multiple porosity levels of 6.9, 7.2 and 7.35 g/cm^3 to characterize porosity effects. Dilatometric samples were carburized and carbonitrided to seven distinct compositions to account for common compositions in the process of thermochemical case hardening heat treatment. The dilatometric samples were rapidly austenitized and quenched and the dilatometric response was evaluated. To fully characterize the martensitic transformation of PM steels, X-ray diffractometry evaluated the amount of retained austenite after quenching. Conclusive results of iterative quenching procedures along with elemental analysis after heat treatment give distinct evidence that PM steels underlie rapid decarburization. This effect ultimately leads to an erroneous evaluation of the martensite transformation kinetics, especially the often proposed effect of porosity on M_S. However, a distinct effect on the accompanied volume change from austenite to martensite is proposed. To account for an interplay of solved carbon and nitrogen, an effective nitrogen contribution of 25% based on carbon equivalent is proposed. Utilizing the effective content, the impact of nitrogen can be projected on carbon within the range of common carbon and nitrogen contents, and a good predictability of the martensite transformation can be achieved. Regarding the resulting hardness, a dependency solely on carbon is suggested. The overall hardness shows a typical maximum at approximately 0.6–0.7 wt%, irrespective of the solved amount of nitrogen.

1. Introduction

Powder-metallurgical (PM) sintered parts are readily used as precision parts in many industrial sectors, especially in engines and transmission [1,2]. In the automotive industry, high mechanical loads must be endured in the PM compo-

* *Corresponding author.*
https://doi.org/10.1016/j.jmrt.2020.05.035

nents, making a subsequent heat treatment obligatory [3,4]. Common case hardening heat treatment procedures consist of an austenitization step (to typically carburize the surface) followed by a subsequent quenching step in a liquid or gaseous medium. An extension of the common carburization sequence is the addition of nitrogen, denoted as carbonitriding. The thermo-chemical heat treatment procedures aim to utilize the chemical gradient to tailor compressive residual stresses along with high hardness close to the surface. Therefore it is necessary to describe the material behavior from the interstitially highly loaded surface through the transition zone up to the chemically unchanged core. High amounts of austenite-stabilizing elements (carbon, nitrogen) extend the transformation time of diffusionally build phases, hence high amounts of martensite can be expected at the surface and near-surface areas.

Martensite is a supersaturated product of athermal transformation from γ-iron. In order to inhibit diffusional decomposition of γ-iron, rapid cooling is necessary to enforce a distorted version of α-iron [5]. The favorable effects of the martensitic phase on the mechanical properties such as yield strength and hardness are undisputed and of great interest for industrial applications. For a full description of the martensite transformation, one needs to evaluate the transformation kinetics with respect to temperature, the amount of retained austenite after quenching and the volume change of the $\gamma \rightarrow \alpha'$ transformation. Nitrogen is analogous to carbon as it is interstitially solved and increases the hardness while also acting as austenite stabilizer which retards thermal and athermal transformation kinetics. The understanding of the impacts of interstitially solved elements on the martensitic transformation and the resulting hardness is crucial for optimizing the carbonitriding process itself, though conclusive work on the interplay of carbon, nitrogen and porosity on the martensitic phase transformation is still lacking in literature.

1.1. *Effects of carbon and nitrogen*

The sole effects of carbon on the martensitic transformation has been under investigation for over a hundred years [6,7]. While a vast amount of literature exists for carbon regarding M_S [8–12], some recent works used artificial neural networks on hundreds of steel compositions focusing on a general prediction model in dependency of the chemical composition of many steels [13,14]. The most prominent model to describe the martensitic transformation behavior was proposed in 1959 by Koistinen and Marburger [15]. In order to predict the final microstructure and residual stress state after quenching, one also needs the prefactor k of the Koistinen-Marburger equation as well as the volumetric change. While the value k was widely reported to be constant with $k = 0.011\,K^{-1}$, more recent assessments suggest that the parameter should also be a function of composition [16]. A linear increasing volume change in dependency of carbon was found for the Fe-C system as well as many common steels [6,17,18]. Only few authors investigated the system of Fe-N in terms of martensitic transformation, reporting for comparable atomic compositions quite similar effects on M_S but significantly lower amounts of retained austenite and a slightly reduced Vickers hardness for the Fe-N system [19,20]. Only few works concentrate on nitrogen and/or combined effects of carbon and nitrogen [21,22], and no conclusive results on the martensitic transformation are reported to this day.

1.2. *Effects of porosity*

Quantitative analysis of the martensitic transformation in PM steels is reported by few authors [23–26], however to date still of great interest, as there is no conclusive work of the impact of porosity on the transformation behavior. Inherent to densities of 6.8–7.4 g/cm^3 are wide areas of open porosity [27,28]. Multiple authors state a shift in the martensite start temperature M_S or the start of diffusional transformation kinetics like bainite as a function of porosity, suggesting a reduced necessary strain energy for transformation due to free surfaces of the pores. For lower densities (higher porosities), M_S is assumed to increase and the incubation time of bainite to be decreased [23–26]. Those increases were reported after a re-austenitization and holding time of 3–5 min at temperatures above A_{c3}. Moreover, an interesting effect on the measured $\gamma \rightarrow \alpha'$ volume change in dependency of porosity was reported by Warke et al. [25]. To summarize, PM steels demonstrate a complex interaction between porosity, the $\gamma \rightarrow \alpha'$ transformation and the resulting microstructure, requiring an intensified scientific attention in order to reach an understanding of the behavior of PM steels in thermo-chemical heat treatment.

1.3. *This work*

This work aims to provide a comprehensive summary of the individual and combined effects of carbon, nitrogen and porosity concerning their interplay on the martensitic phase transformation in the low alloy PM-steel Astaloy 85Mo. For this purpose, three porosity levels at seven combinations of carbon and nitrogen were investigated by high-speed induction dilatometry, X-ray diffractometry and metallography. Models to predict the transformation kinetics and resulting hardness are proposed and discussed with respect to literature. Dilatation curves of iterative heating-quenching procedures visualize the transition of apparent M_S temperature and shed light on the effects of porosity on the transformation kinetics. Finally, the interplay of carbon and nitrogen concerning the resulting microstructure and hardness is elaborated.

2. Material

Water-atomized and pre-alloyed powder Astaloy 85Mo was used as base material for this work. Compacting and sintering conditions were adjusted to result in average densities of 6.9, 7.2 and 7.35 g/cm^3, respectively. By addition of graphite, the alloy was modified to a base carbon content of 0.3 wt%. Combustion analysis of the sintered state confirmed a fairly high oxygen content of 0.2 wt%. Dilatometric samples were machined and subsequently carbonitrided to selected compositions of carbon and nitrogen. The carbonitriding was carried out at 940 °C, controlling the propane (C_3H_8) and ammonia (NH_3) addition to result in the desired composition. The alloy compositions are depicted in Fig. 1 and also listed in Table 1, for convenience. The selected compositions were chosen based

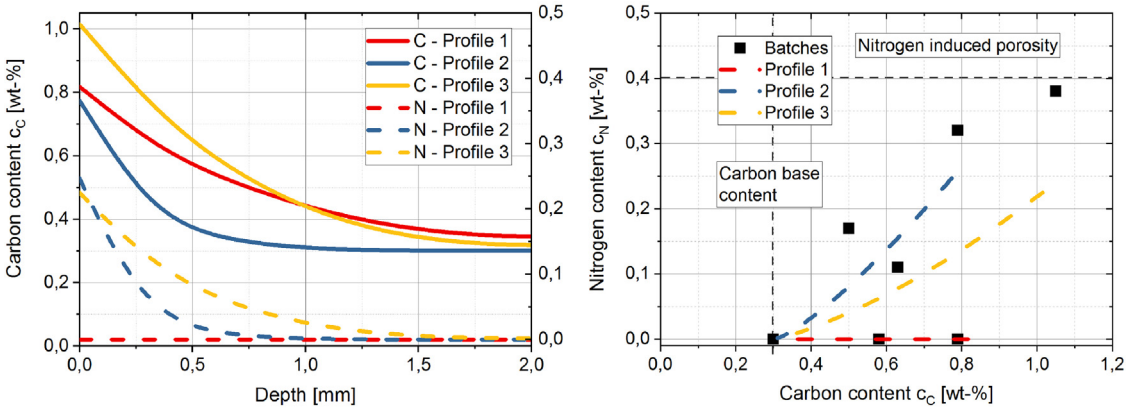

Fig. 1 – Plot of investigated batches and their distribution in a carbon-nitrogen-diagram. Left: Typical technological concentrations of C/N and depth profiles extracted from [22] and right: their carbon nitrogen combinations as dashed lines. The black dots refer to the investigated compositions in this work.

Table 1 – Chemical composition of the investigated the carbonitrided batches.

Batch	C [wt%]	N [wt%]
0.3C-0N	0.30	–
0.58C-0N	0.58	–
0.79C-0N	0.79	–
0.5C-0.17N	0.5	0.17
0.63C-0.11N	0.63	0.11
0.79C-0.32N	0.79	0.32
1.05C-0.38N	1.05	0.38

on common combinations of carbon and nitrogen in depth profiles. For clarification, Fig. 1 shows common carbonitriding depth profiles (left) and the resulting combinations of carbon and nitrogen with the selected compositions (right). The batch reference points were chosen in a wider scope so that the whole range of possible carbonitriding procedures is covered by the experiments.

Three batches were carburized (0.3C-0N, 0.58C-0N, 0.79C-0N) in order to isolate the effects of carbon. Furthermore, three more batches are in a typical combination of carbon nitrogen to investigate (0.5C-0.17N, 0.63C-0.11N, 0.79C-0.32N). The last batch is excessively loaded with solute interstitials (1.05C-038N) in order to investigate a possible, limiting effect on the transformation. The chemical composition was measured by glow discharge optimal emission (GDOES) analysis and is given in Table 1. The microstructure of the batches after carbonitriding was martensitic (along with retained austenite) and therefore no coarse precipitates were whether expected nor detected by metallography.

3. Methods

3.1. *Dilatometry*

Dilatometry is an established technique to precisely measure the length change of a metallic sample with changing temperature [29,30]. The specimen geometry is a hollow cylinder with an outer diameter of 4 mm and inner diameter with 3 mm and a length of 10 mm and is heated via induction and the temperature is controlled by a thermocouple type S. Measurements were performed using one thermocouple in the center of the specimen. To avoid possible influences due to oxidation, the measurement setup is enclosed in a vacuum chamber. An atmospheric pressure of 10^{-1} mbar was adjusted, followed by flooding with He to 0.8 bar to exclude oxidation as well as lesser decarburization/denitridization effects in the heat treatment procedure. The specimens are heated to an austenitizing temperature of 940 °C in 10 s and are held for 10 s. This "rapid" austenitization procedure was performed as the open porosity of the sinter steel shows rapid decarburization under vacuum atmosphere (which will be discussed in Section 5). Rapid austenitization was sufficient for homogenization since the microstructure did not show coarse precipitates, hence a longer austenitization time is unnecessary [31]. This has been validated for common low alloy steels [32]. The rapid cooling from austenitizing temperature to the desired temperature is accomplished in 2 s with He, preventing a preliminary transformation of the ferritic, pearlitic or bainitic phase.

3.2. *BET measurement*

The Brunauer-Emmett-Teller (BET) theory explains the adsorption of gaseous molecules on solid surfaces and can be used as analysis technique to determine the specific surface area of a solid material. More information about the measurement can be found in [33]. This is especially important to understand the diffusional process of porous steels, since open porosity acts as a diffusion channel into the depths of the heat treated samples. BET measurements were carried out according to ASTM Standard D4780 [51] using Krypton at 77K. The investigated densities of 6.9/7.2/7.35 g/cm^3 were analyzed on three samples each. In Table 3 the values of the measurement are shown.

3.3. *Thermal etching and microscopy*

In order to analyze the prior austenite grain size at different austenitization temperatures it is necessary to reveal

the austenite grain boundaries. There are different methods which make an investigation of the austenite grain boundaries possible. In [34] it is shown that the method of thermal etching provides the best results for a metallographic determination of the austenite grain boundaries. Thermal etching reveals the austenite grain boundaries in a pre-polished sample by grooves that emerge at the intersections of the austenitic grains. Hereby it utilizes the high diffusion coefficients of surface diffusion in comparison to volume diffusion, making the prior austenite grain sizes visible at room temperature under the optical microscope [35]. Thermal etching was executed with the same dilatometric sample set and sample geometry. Before the thermal etching the dilatometry specimen had been ground to receive a small flat surface, which facilitates a microscopic investigation. Finally, they were polished with 1 μm diamond paste. The austenitizing step was identical as explained in Section 3.1. To avoid a martensitic transformation the samples were cooled down with 1 K/s after the austenitization. The evaluation of the grain sizes was carried out with binarized images of scanning electron micrographs (see [30] for more details). Austenite grain sizes were determined with the linear intercept method according to DIN EN ISO 643. Measured austenite grain sizes of $\delta_{6.9} = 11.0 \pm 0.1\,\mu m$, $\delta_{7.2} = 10.5 \pm 0.4\,\mu m$ and $\delta_{7.35} = 10.3 \pm 0.1\,\mu m$ were identical for all porosity levels. The relatively fine grains are common for PM steels, as the finely dispersed pores act as austenitic grain boundaries, thus limiting the growth depending on the pore distribution.

3.4. *Hardness measurements*

For microstructural analysis, the cut plane was perpendicular to the axis with the cut position in the middle of the sample. Given samples were ground and finally polished with 1 μm diamond paste. Vickers hardness testing was performed on a Qness Q30a+ micro hardness tester with forces of 0.1 kg (HV0.1) and 10 kg (HV10) according to DIN EN ISO 6507-1 [36]. As PM steels show finely distributed pores, the HV0.1 indentations were selected manually in pore-free areas in order to measure the pore-free material response.

3.5. *X-ray diffractometry*

X-ray diffractometry was performed for analysis of retained austenite according to ASTM standard E975 [37] utilizing the 6 peak fit of the martensite interference lines $\{200\}_\alpha$, $\{211\}_\alpha$ and $\{321\}_\alpha$, as well as austenite interference lines $\{200\}_\gamma$, $\{220\}_\gamma$ and $\{311\}_\gamma$. The profiles were measured in $2\Theta = 0.1°$ with MoKα radiation on three samples for each composition. The samples were electropolished to exclude possible mechanical effects on retained austenite and were measured in the center of the dilatometric sample.

4. Results

4.1. *Analysis*

The martensitic transformation kinetic is known to be athermal. While mathematical models to describe phase transformations exist for a long time, one of the most utilized models with respect to temperature is the Koistinen-Marburger equation [15]

$$w_M^{KM} = 1 - \exp(-k \cdot (M_S - T)) \tag{1}$$

with M_S being the martensite start temperature (in °C or K, respectively) and a prefactor k in 1/K. As this only predicts the phase change from typically austenite to martensite, the volume change from fcc to bcc has to be considered. One should keep in mind that the volumetric change from fcc to bcc is dependent on the temperature, and therefore a reference temperature T_{ref} must be defined for comparability. In our work we set the reference temperature for each composition to $T_{ref} = M_S$. The martensitic volume change is also dependent on the composition, especially on interstitially solved carbon and nitrogen. The interplay between the prefactor k and the volumetric change of the austenite decomposition can be ambiguous, as multiple combinations of k and $\Delta V_{\gamma \to \alpha'}$ can lead to similar quantities of length change. Therefore, the kinetic parameters M_S and k are chosen so that the transformation start temperature and the amount of predicted retained austenite at room temperature is in accordance with experimental data. The volume change is subsequently determined to fit the experimental curve.

4.2. *Transformation kinetics*

As it is challenging to visualize the co-dependency of carbon and nitrogen, a simplification is proposed. An effective content c_{eff} is defined with a bilinear dependency on the carbon and nitrogen content. The effect of nitrogen on the transformation kinetics is then given as an effective ratio related to the carbon content

$$c_{eff} = c_C + A \cdot c_N \tag{2}$$

with c_C and c_N being the element contents in wt%. Therefore we impose an effective content as a superposition of the carbon content A of the nitrogen content on the x-axis. The martensite start temperatures seen in Fig. 2a show a known linear decrease in dependence of the interstitial alloy content. The squares refer to carburized and the dots to carbonitrided compositions, while the color refers to the state of porosity. The evaluated M_S values are shown for all porosities and compositions. No significant trend of the porosity on M_S can be evaluated considering the standard deviations (and will be discussed in detail in Section 5). The black symbols are the summarized values for each composition. We impose an effective factor of $A = 0.25$ to account for the effect of nitrogen in comparison to carbon. The effective content does hereby also lead to a good overall description of the dependency of nitrogen. The M_S temperature of the initial state with 0.3C-0.0N begins at 379 °C and linearly decreases to 130 °C for 1.05C-0.38N. The standard deviations calculated through the best fits of 5 samples vary by $\Delta M_S = \pm 4$ K for 0.3C-0.0N up to $\Delta M_S = \pm 20$ K for 0.5C-0.17N. With the effective content approach, a good predictability is given.

The choice of reasonable values of the prefactor k is dependent on the amount of retained austenite and the value of M_S

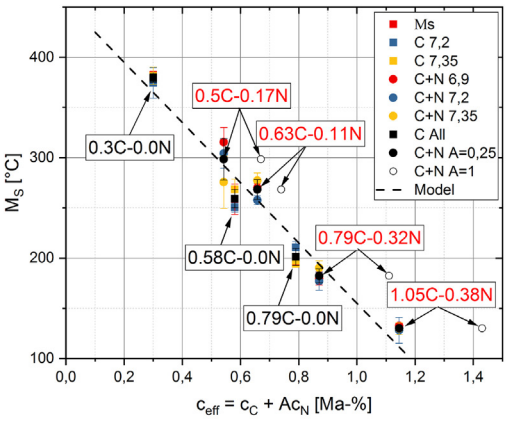

(a) Martensite start temperatures in depenceny of the effective content of carbon and nitrogen. A stands for the effective multiplyer of nitrogen referred to carbon.

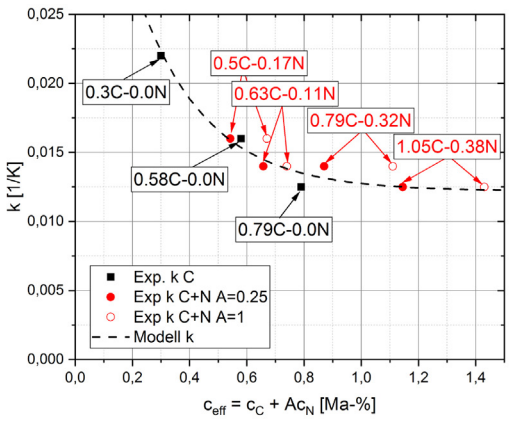

(b) Evaluated values for the prefactor k in dependency of the effective total content of carbon and nitrogen. A stands for the effective multiplyer of nitrogen referred to carbon.

Fig. 2 – Kinetic parameters M_S and k in dependency of the effective content c_{eff}. Carbonitrided batches are shown with two multipliers A = 1 (hollow circles) and A = 0.25 (full circles). With a multiplier of 1, the plot shows the cumulative wt% of both species. Regarding the effect on the transformation kinetics, the best fit to describe the transformation kinetics is with A = 0.25.

and must be derived from experimental data. A combination of linear fit for M_S and decreasing exponential fit for k provides a good agreement between experimental data and the model with

$$M_S[^\circ C] = 455 - 300 \cdot c_{eff} = 455 - 300 \cdot c_c - 75 \cdot c_n \quad (3)$$

$$k[1/K] = 0.0122 + 0.01 \cdot \exp\left(-\frac{c_{eff} - 0.303}{0.24}\right). \quad (4)$$

By inserting the dependencies of M_S and k in Eq. (1), the amount of retained austenite in dependency of c_{eff} can be calculated and will be discussed in the next section.

4.3. *Retained austenite*

The exponential part of the Koistinen-Marburger equation can be interpreted as the amount of retained austenite at the final quench temperature $T = 20\,^\circ C$

$$w_A^{KM} = \exp\left(-k(c_{eff}) \cdot \left(M_S(c_{eff}) - T\right)\right). \quad (5)$$

The following plot (see Fig. 3) depicts the retained austenite contents of the investigated batches over the effective content along with the predicted amount of retained austenite.

Retained austenite contents for the batches below $c_{eff} = 0.6$ wt% were below a reliable analysis range in the XRD analysis of 3 vol% and therefore show high standard deviations with respect to the measured value and should be interpreted with caution. Retained austenite contents exponentially rise with increasing carbon and/or nitrogen content up to 25% for 1.05C-0.38N and can be predicted with a overall good agreement for all combinations of carbon and nitrogen.

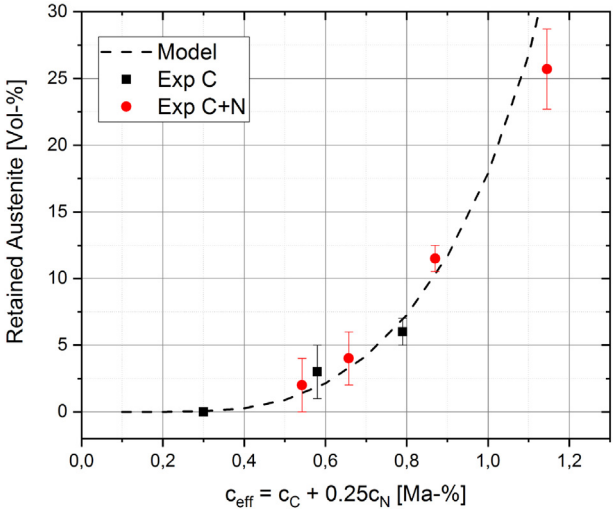

Fig. 3 – Retained austenite contents in dependency of the effective content of carbon and nitrogen.

4.4. *$\gamma - \alpha'$ volume change*

The martensitic transformation is accompanied by a volume change that is dependent on the amount of carbon solved in the prior austenitic phase. The volumetric change from austenite to martensite with respect to temperature is evaluated according to [6] with

$$\left(\frac{\Delta V_{\gamma\to\alpha}}{\Delta V_\gamma}\right)_T = 3\left(\frac{\Delta L_T}{L_\gamma(T)}\right) + 3\left(\frac{\Delta L_T}{L_\gamma(T)}\right)^2 + \left(\frac{\Delta L_T}{L_\gamma(T)}\right)^3 \quad (6)$$

where ΔL_T refers to the difference in length between the α and γ phase at temperature T, and L_γ to the total length of the sample in γ phase at the respective temperature. Evaluation temperature was set to M_s for each composition to increase

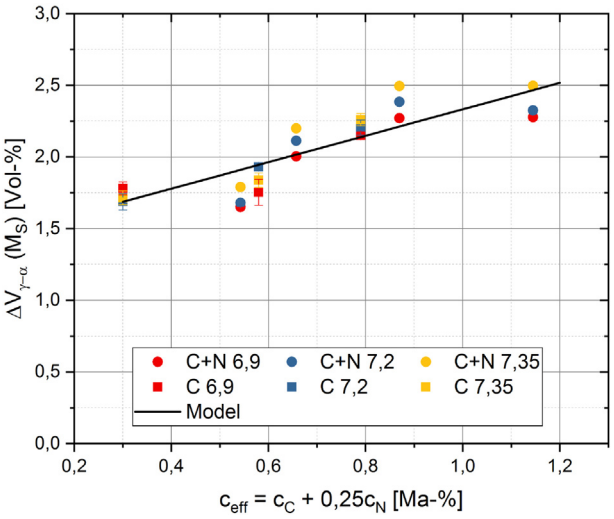

Fig. 4 – The $\gamma \rightarrow \alpha'$ volume change accompanied by the martensitic transformation, evaluated at reference temperature M_S for each composition, in dependency of effective total content.

comparability to other works [6,17,38]. In the evaluation the amount of retained austenite was considered and corrected for the partial martensite transformation accordingly (see Section 4.3). An increasing $\gamma \rightarrow \alpha'$ volume change with respect to the overall content is illustrated in Fig. 4. In contrast to results presented before, a dependency of the porosity is evident especially in the C+N compositions.

Data points illustrated as squares refer to carburized compositions without nitrogen. An increasing volume change with respect to carbon and nitrogen leads to an overall volume change from 1.5 vol% up to 3.0 vol%. A good agreement with a linear increasing function with

$$\Delta V_{\gamma-\alpha}(M_s) = 1.41 + 0.9225 \cdot c_{eff} \tag{7}$$

with respect to the effective content is given. Focusing on the nitrogen-containing batches, the question arises how the combination of carbon and nitrogen affects the resulting volume change.

4.5. *Hardness*

Vickers hardness HV0.1 measurements (see Fig. 5a) did show no deviations between the densities, since the indentation is too small to be influenced by porosity. For identical chemical composition and heat treatment, identical hardness values are expected and were measured in this work. The carburized compositions (Fe-0.3C, Fe-0.58C and Fe-0.79C) result in higher hardness values in comparison to the Fe-C-N alloys. However, a plateau is approximately found at $c_c = 0.6–0.8$ wt%. While the carburized batches tend to higher hardness values, a lower hardness is found for the Fe-C-N compositions. In comparison to HV10, a significant decrease in overall hardness due to porosity is depicted, while the hardness shows the same overall trend in dependency on the effective content c_{eff}.

Higher standard deviations in HV0.1 were found for the carbonitrided samples (ΔHV = 70–100 HV0.1) in comparison to the carburized samples (ΔHV = 30–50 HV0.1). A microhardness hardness formula can be given with a quadratic approach

$$HV0.1 = 2648 \cdot c_c - 1609 \cdot c_c^2 \tag{8}$$

in dependency of carbon content only, and for the macrohardness, including porosity with

$$HV10 = 137 + 1566 \cdot c_c - 878 \cdot c_c^2 - 19 \cdot p \tag{9}$$

with $p = (\rho_0 - \rho)/\rho_0$. The course of the hardness development with respect to the effective content resembles a typical increasing hardness plot, and the decrease of overall hardness in a carbon region of $c_{eff} \geq 1.0$ wt% is not significant.

The demonstrated results can be predicted with the effective contents and presented models. Now the question arises if the presented results (summed up in (Table 2)) can be verified by literature, which will be done in the next section.

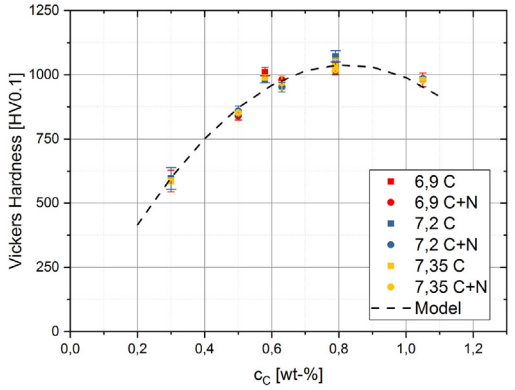

(a) [Vickers hardness HV0.1 measurements with respect to the carbon content c_c.

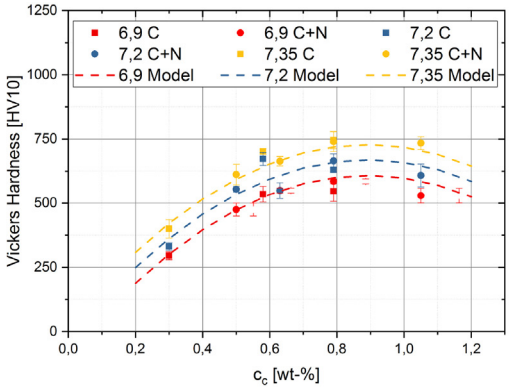

(b) Vickers hardness HV10 measurements with respect to the carbon content c_c.

Fig. 5 – Left: Micro-hardness HV0.1 with respect to carbon composition for all porosities. Right: Macro-hardness HV10 measurements with respect to carbon. While the micro-hardness is independent of porosity, the macro-hardness shows three distinctive curves in dependency of porosity.

Table 2 – Martensite transformation parameters summarized with standard deviations.

Batch	M_S [°C]	k [1/K]	RA [vol%]	$\Delta V_{\gamma\to\alpha'}$ [vol%] ($\rho = 6.9$ g/cm^3)	$\Delta V_{\gamma\to\alpha'}$ [vol%] ($\rho = 7.2$ g/cm^3)	$\Delta V_{\gamma\to\alpha'}$ [vol%] ($\rho = 7.35$ g/cm^3)
0.3C-0N	379 ± 4	0.022	–	1.78 ± 0.5	1.688 ± 0.1	1.71 ± 0.1
0.58C-0N	259 ± 9	0.016	–	1.75 ± 0.2	1.93 ± 0.1	1.84 ± 0.1
0.79C-0N	201 ± 8	0.0125	6 ± 1	2.15 ± 0.1	2.2 ± 0.1	2.26 ± 0.1
0.5C-0.17N	298 ± 20	0.016	2.4 ± 1	1.65 ± 0.2	1.68 ± 0.2	1.79 ± 0.2
0.63C-0.11N	268 ± 10	0.014	4 ± 1	2.00 ± 0.4	2.11 ± 0.2	2.20 ± 0.2
0.79C-0.32N	182 ± 7	0.014	11.5 ± 1	2.27 ± 0.3	2.38 ± 0.3	2.49 ± 0.6
1.05C-0.38N	130 ± 2	0.0125	25.7 ± 3	2.28 ± 0.2	2.32 ± 0.2	2.50 ± 0.3

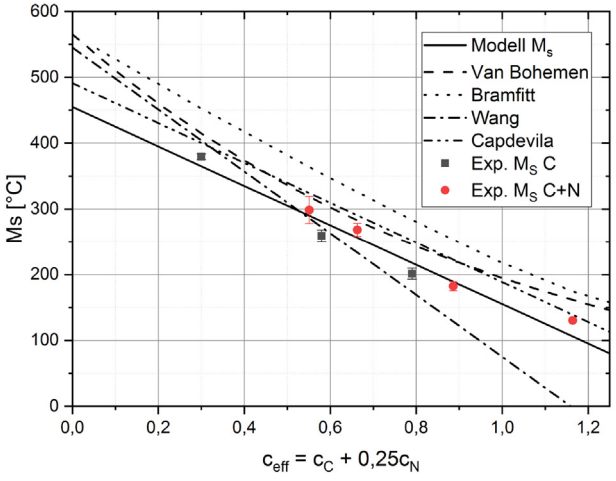

Fig. 6 – Martensite start values in dependency of the overall effective content c_{eff} compared to literature data of [13,39–41] in dependency of solely carbon.

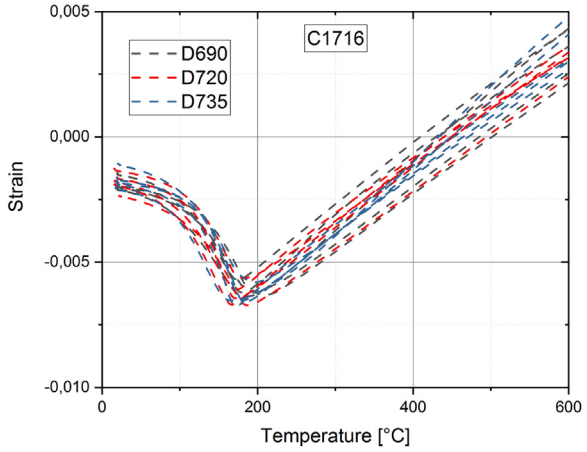

Fig. 7 – Plot of all dilatation experiments of the batch C1716 in multiple porosity states of 6.9 g/cm^3, 7.2 g/cm^3 and 7.35 g/cm^3.

5. Discussion

5.1. *Martensite start*

5.1.1. *Carbon nitrogen dependency*

Despite the vast amount of research done on the influence of carbon content on M_S [39–41], new work by Capdevila et al. [13] using neural networks on literature data can be used as reference data within this work. Those approaches seem reasonable as the amount of investigated compositions can give comprehensive dependencies of M_S. In 2012 van Bohemen [41] suggested an exponential dependency of carbon on the prefactor k as well as on M_s. In the following Fig. 6, our data is compared to the literature approaches.

A reasonable overall decrease of M_S with the amount of solved interstitials is given. In total, the measurement results lay within the variety of proposed carbon dependent models. The diminished effect of nitrogen in comparison to carbon fits well compared to literature models. Comparing the M_S temperature carburizing state of 0.79C-0.0N with the carbonitrided state 0.79C-0.32N, the diminished effect of nitrogen can be elaborated. With an increase of 0.32 wt% N, M_S decreases by 16 K, therefore an diminished effect of nitrogen in comparison to carbon is evident. In contradiction, Prenosil [42] reports an effect of nitrogen on M_S of $\Delta M_S = 180$ K/wt% while in this work we have a reduced effect of $\Delta M_S = 75$ K/wt%. Also, compared to other carbonitrided steels, significantly reduced values of retained austenite are reported in this work. On the other hand, the retained austenite values are in agreement with results of pure iron. The question arises to what extent the alloy system influences the effect of nitrogen in the martensitic transformation.

5.1.2. *Porosity dependency of M_s*

Multiple authors have stated a strong dependency of the martensite start temperature on the porosity state [25,43]. This statement cannot be supported by our data of more than 150 continuous cooling tests, and in the following the discrepancies will be elaborated. In Fig. 7 all analyzed samples of batch C1716 (5 samples a 3 porosities) are shown. The data indicate a small scattering of the martensite start values in the usual set of ranges, since not all samples are perfectly homogeneous in their composition. Yang and Bhadeshia [44] stated that, depending on the method of evaluation, inevitable standard deviations of $\Delta M_S \pm 6$–12 K occur, hence an effect of porosity can hardly be identified nor a statistically sound distinction can be found.

Auxilliary tests on the heating of dilatometric samples were performed with different holding times, showing rapid decarburization while austenitizing. The BET measurements regarding the diffusionally active surface along with element measurements of samples austenitized for 10 min are shown in Table 3. A notable decarburization can be found for both investigated batches and all porosities. Interestingly, the

Table 3 – Data of the BET measurements and geometrical approximation of the surface. The ratio is the quotient of the measured, effective surface divided by the geometrical surface. The decarburization was measured for two batches Fe-0.3C-0N and Fe-0.5C-0.17N after a heat treatment of 10 min at 940 °C.

Density	Geometric surf. [m²]	Measured BET surf. [m²]	Ratio	Δc_c Fe-0.3C-0N [Δwt%]	Δc_c Fe-0.50C-0.17N [Δwt%]
6.9	0.0018	0.631	350	−0.073	−0.225
7.2	0.0018	0.526	292	−0.077	−0.155
7.35	0.0018	0.393	219	−0.048	−0.141

decarburization was significantly higher in Fe-0.5C-0.17N in comparison to Fe-0.3C-0N (which is attributed to the higher carbon potential, leading to potentially higher mass transfer rates), though a quantification of the decarburization is not reasonable since every sample inhibits discrepancies in sample homogeneity and porosity architecture.

This is even more the case for thin dilatometric samples with 0.5 mm wall thickness (as used in this work), that are typically used to ensure homogeneous distribution through carburization and/or carbonitriding. For the following discussion the reader should keep in mind that the porosity architecture of PM steels is open and also connected [4,27,28] and therefore leads to dramatically increased activity of the investigated component with the ambient atmosphere. Thus, with increasing porosity, the amount of diffusional activated areas is increasing exponentially, as not only the amount of pores does increase, but also their interconnectivity to deeper areas of the investigated specimens.

Fig. 8a shows the dilatation curve of undercooled, austenitized samples. While a short austenitization of 10 s did lead to identical martensite start temperatures of 184 °C and 187 °C, a significant shift of the 180 s austenitized samples to 205 °C and 210 °C is evident. We did also detect a higher standard deviation between samples of longer austenitization times, as fluctuations in porosity morphology can lead to unsteady decarburization levels, thus resulting in not only an erroneous determination of M_S but also decreasing statistical precision. For long austenitization times of 1800 s, an apparent severe increase of M_S to 350 °C, results in an erroneous determination of $\Delta M_s \approx 170$ K. Fig. 8b shows the effect of the austenitization time on the martensite start temperature. In the sequence of heating, annealing effects of the formerly martensitic microstructure can be seen. The increase of measured M_S after 1800 s is $\Delta M_S = 170$ K, after 2400 s $\Delta M_S = 190$ °C, 2700 s $\Delta M_S = 210$ °C and 2880 s $\Delta M_S = 220$ °C. Considering that the diffusionally activated surface is 200–300 higher than for conventionally cast samples, and that this surface is also connected to deeper areas of dilatometric samples, decarburization provides a reasonable explanation. Furthermore, the volume change accompanied with the martensitic transformation reduces with every reaustenitization step and the annealing effects are barely visible in comparison to the first cycle. One could argue that the austenitization time was not sufficient to completely solve the carbon and nitrogen in austenite. Fundamental work of [31] and also work of Miokovic et al. [32] did prove that rapid austenitization to 900–1000 °C in few seconds is capable of fully solving the carbon in many steels, and we assume that this is also the case for nitrogen. Another argument is the shift of M_s. As carbon and nitrogen are known to stabilize austenite (and therefore reduce M_S when solved), the one heat treatment resulting in the lowest value of M_s can be identified as the maximum amount of solved carbon and nitrogen.

5.2. *The parameter k and retained austenite*

As mentioned before, the parameter k is fit along with M_S to predict the amount of retained austenite after quenching to

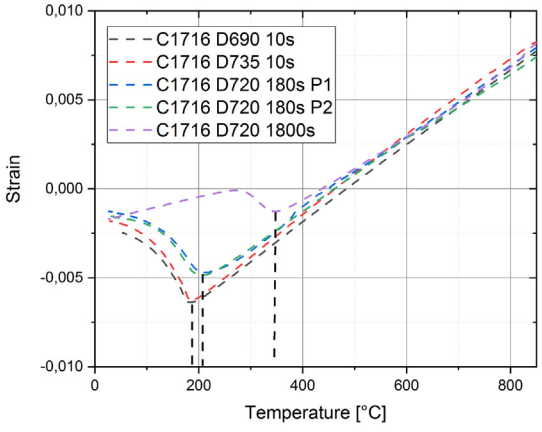

(a) Strain vs. Temperature of multiple austenitization times with a significant shift in M_S in dependency of the duration of austenitization. Identical heat treated samples show reproducable M_S values, while the a change in the duration leads to a significant change in M_S

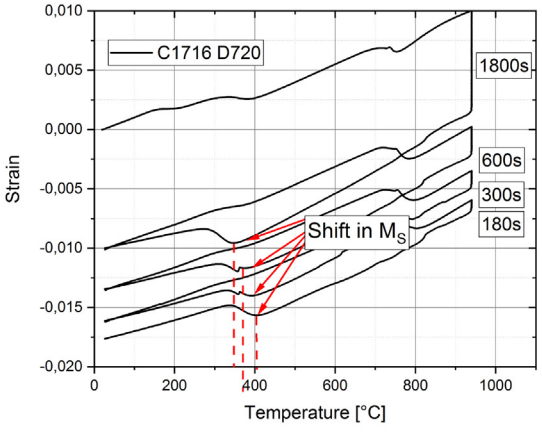

(b) Strain vs. Temperature for Fe-0.79C-0.32N sample of density 7.2 gcm^{-3} in subsequent heat treatment steps. The apparent martensite start temperature of the transformation is increasing with an addition of the austenitization time.

Fig. 8 – The dilatation curves with respect to temperature of batch Fe-0.79C-0.32N (C1716), left: multiple dilatation curves of samples with respect to austenitization times. The correctly determined value is $M_S = 180°$. Right: Dilatation curve of one sample in a subsequent heat treatment procedure to visualize the shift in M_S with longer austenitization times.

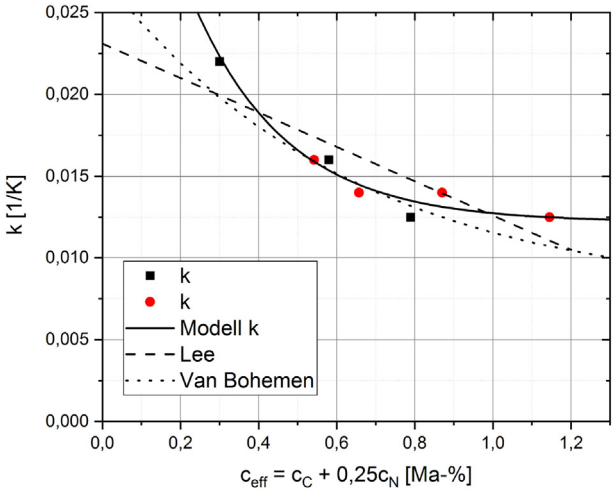

Fig. 9 – Comparison of the prefactor *k* for the investigated compositions with literature data for carbon [8,9].

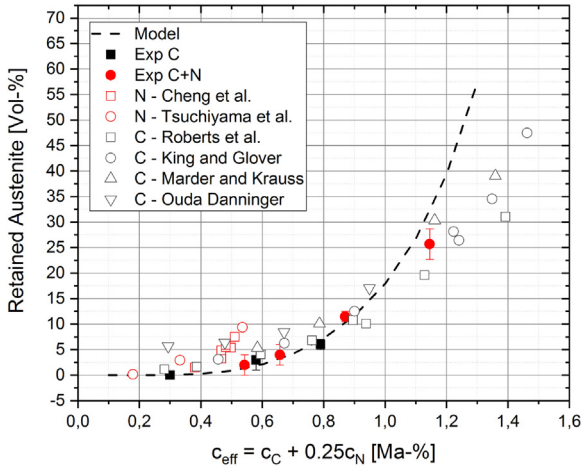

Fig. 10 – Retained austenite values measured by x-ray diffractography in comparison to literature of Fe-C alloys (black, [45–48]) and Fe-N alloys (red [19,20]).

RT. While some of the older literature suggested a constant value of $k = 0.011$, some recent works reported a dependency on alloy content like Lee [9] $k_{Lee} = 0.0231 - 0.0105c_c$. Van Bohemen [8] investigated a low alloy steel carburized in multiple carbon compositions (%C = 0.46, 0.66, 0.80) and indicated an exponential dependency of the prefactor *k*. The proposed model of Lee as well as the experimental values of van Bohemen are shown in Fig. 9. For the compositions with carbon individually, a good comparability can be found between the relations in this work compared to the literature review.

For combined effects of carbon and nitrogen, the picture is increasingly complex. For compositions with high carbon/nitrogen contents of $c_{eff} = 0.8$ wt% and more, a plateau of the prefactor *k* at approximately $k = 0.0125$ can be defined. This gives confidence that the exponential approach suggested is reasonable, while a linear approach seems only to be applicable in a narrow field of low alloy steels between $c_c = 0.4$–0.7. Comparing the fit function for retained austenite with literature, a good agreement of the experiments is given for the Fe-C alloys. 10 To evaluate possible effects of porosity, the data of Ouda et al. [48] is shown. The evaluation was performed with magnetic measurements (that can be ambiguous, see [48]), but were validated by Rietfeldt Analysis for 1 wt%C with an amount of retained austenite of 17% that fit well with our modeling approach. For low carbon contents, the amounts of measured retained austenite seem overestimated. The Fe-N data for retained austenite was added and the factor 0.25 was superimposed for comparability. For Fe-N steels, the factor of 0.25 seems to underestimate the effective impact of nitrogen. For example, for an effective content of $c_{eff} = 0.56$ wt% 2.5 vol% of retained austenite are proposed, while literature states values of 7.5–10.0 vol%. It can be stated that the combined effect of carbon and nitrogen on a low alloyed steel cannot be calculated by a mixture-rule. Further investigations seem reasonable to understand the influence factors of cooperatively solved carbon and nitrogen, and how the interaction of both play a role in the development of retained austenite.

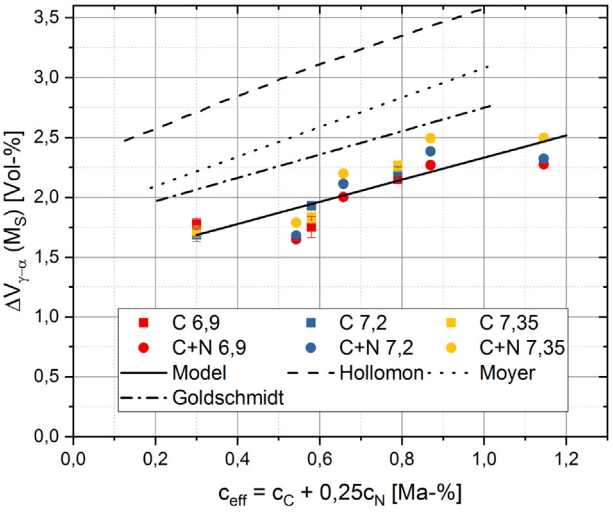

Fig. 11 – The associated volume change of martensite with respect to effective content in comparison to literature [6,17,18].

5.2.1. *$\gamma - \alpha'$ volume change*

The volume change associated with the martensitic transformation is known to be increasing with interstitially solved carbon. Similar observations are found in Fig. 11 in dependency of the effective carbon content. A good agreement with a linear increasing function with respect to the effective content is given. It should be noted that the literature curves are referred to carbon only, since no reliable data for nitrogen was found up to date. Cheng et al. [19] presents constants for Fe-N martensites, indicating that the volume change of nitrogen martensite should result in higher volume changes compared to typical Fe-C martensite. When investigating the carbonitrided batches referred to by dots, no distinctive increase of the volume change in dependency of nitrogen is found. On the contrary, a slight nonlinearity of batches with both carbon and nitrogen seems to be given. However, the differences are small,

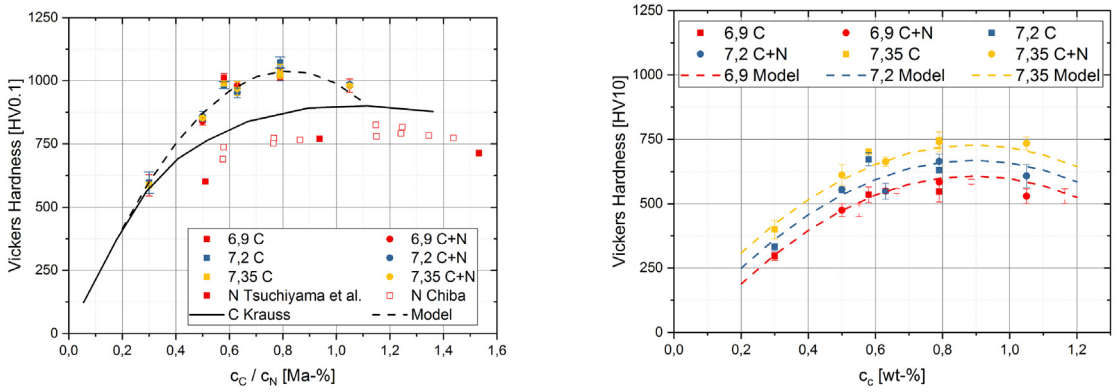

(a) Hardness HV0.1 measurements in dependency of solely carbon or nitrogen content.

(b) Hardness HV10 measurements in dependency of solely carbon content c_c.

Fig. 12 – Vickers hardness tests of all investigated batches in dependency of element composition and porosity. Left: Micro-hardness HV0.1 in dependency of solely carbon, right: macro-hardness HV10 measurements with three distinctive slopes in dependency of porosity.

and the decreasing effect of the highly carbonitrided batch ($c_{eff} = 1.15$) could be affected by the rising amount of retained austenite. Overall, utilizing a linear fit a good prediction can be made for a wide variation of carbon and nitrogen. While the increasing trend describes the same slope as found in literature (dependent on carbon), a notable offset exists for all compositions and porosity levels. As we furthermore find a distinctive sequence for the three porosity states, we assume that porosity could play a role in the resulting volume change of the sample. For 5 of 7 investigated compositions, the samples with highest densities (yellow) also result in the highest measured volume changes, while in 6 of 7 compositions, the samples with highest porosity (red) show also the least volume change. The indications justify the assumption that porosity can be held accountable for the decrease in overall transformation volume change, as a finely distributed porosity can act as stress relief in the microstructure, hence the share of mechanical stabilization of austenite is decreased. The overall difference between the porosity levels is however small, and differentiating model approach seems not reasonable on the given data. For the future, bulk material should be added in order to quantify porosity effects on the volume change.

The free surface between the pores and the material can act as possible nucleation site for martensite, as the necessary strain energy is reduced. This could be an explanation of an apparently reduced volume change of the sample. Other authors like Warke et al. [25] have found similar effects, reporting a decreasing volume change from $\gamma \rightarrow \alpha'$ dependent on the porosity. Follow-up work is necessary to shed light on the mechanisms of martensitic transformation in porous steels.

5.3. *Hardness*

Vickers hardness tests with force of 0.1 kg were carried out in order to rule out effects of porosity due to small indentations, and furthermore tests with 10 kg for a combined effect of hardened microstructure and porosity. Measurements of HV1 were not reasonable as the area of indentation would only include several pores, making it vulnerable to statistical errors. It should be noted that the indentations of HV10 measurements do not fulfill DIN EN ISO 6507 [36], as the distance to the sample surface is approximately one length of the diameter (compared to 2.5 times referring to the standard). However, a good tendency between the porosities can be seen in the data. The presented hardness values are significantly higher compared to data reported by Krauss et al. [49]. The increased hardness can be explained by a reduced influence of selftempering, as the small dilatometric samples were quenched in less than 2 s. For slower cooling times, a reduced hardness due to selftempering is expected. The second mechanism leading to a hardness increase is based the size of prior austenite grains and the resulting microstructure. It is known for PM steels to result in high microhardness. Data of Tsuchiyama [20] and Chiba [50] suggests an analogous trend for the Fe-N alloys, but at lower overall hardness levels. The depiction in dependency of carbon can furthermore be justified when investigating the carbonitrided compositions and solely carbon in Fig. 12a. While Fe-0.58C-0N results in a micro-hardness of approx. 1000HV0.1 the Fe-0.63C-0.11N composition does not result in higher but even lower hardness values. The same is apparent for Fe-0.79C-0N and Fe-0.79C-0.32N, with comparable hardness values, even though the amount of nitrogen is highly increased.

The Fe-1.05C-0.38N has good overall hardness even though high amounts of interstitial elements are solved. Interestingly, with increasing nitrogen content the overall hardness does not increase. For the reported data with nitrogen contents of less than a half of carbon, it can be stated that the hardening increase of nitrogen is neglectable compared to carbon. In Fig. 12 a reasonable trend in dependency of solved carbon is given, though this trend could change when the ratio of nitrogen compared to carbon increases.

6. Conclusion

Dilatometer samples were carburized and carbonitridied and investigated by dilatometry, metallography and XRD. Multiple density levels of 6.9, 7.2 and 7.35 g/cm^3 were analyzed to inves-

tigate porosity effects. Samples were quenched with 500 K/s in order to suppress diffusionally driven transformations. Iterative austenitization procedures confirmed an influence of the austenitization time on the transformation behavior. Oxygen contents of 0.2 wt% found in sintered samples along with the decarburization phenomena indicte that the sintering and/or carbonitriding still have to be optimized, therefore the results should be regarded as preliminary. Concerning the heat treatment procedure for PM steels, the following summary can be drawn:

- In contrast to literature, no porosity effect was found on the transformation kinetics (M_s, k). On the contrary, a strong tendency to decarburization of PM steels is demonstrated. Elemental analysis of austenitized samples confirmed severe decarburization the samples, explaining the shift of M_S in the literature. This can be attributed to the open porosity of PM steels, especially the significantly increased surface. BET measurements confirmed a 200–300 times higher diffusionally activated surface compared to the geometrical surface, exponentially rising with increased porosity.
- With the effect of rapid decarburization in dependency of porosity (intrinsically due to increased surface), the effect of increased M_S with increasing porosity can be confirmed by repeated quenching procedures. A strong depletion of carbon even in deep areas of the sample occurs due to the open porosity. This depletion finally leads to an apparent increase in the M_S temperature.
- Rapid heat treatment of PM steels is necessary in order to investigate transformation effects of an unaffected composition. To ensure a homogeneous solute, preceding microstructural analysis must confirm fine microstructural features, so that a rapid austenitization can dissolve carbon or carbon-nitrogen precipitates.

The relevant factors for the Koistinen-Marburger equation (M_s, k and the resulting amount of retained austenite), the volume change accompanied by the martensite transformation and the resulting hardness were evaluated, mathematical relations are proposed and a discussion regarding validity of measured data was carried out. The essential findings are listed in the following:

- To account for the effect of interstitial nitrogen on martensitic transformation, an effective content $c_{eff} = c_c + 0.25c_n$ was proposed. The diminished effect of 25% in comparison with carbon was chosen as it predicts the martensitic transformation behavior both of solely carburized and carbonitrided samples. This is in contradiction to work of Prenosil [42], reporting an effect of 60%.
- A linear dependency of the effective content on M_S provides a good agreement with experimental data. The same applies for the prefactor k, which was modeled with an exponential approach. The resulting calculated amounts of retained austenite are also in good agreement with the experiments. The proposed models agree with established equations in the literature review.
- A linear dependency of the transformation volume change to martensite with respect to carbon and nitrogen is proposed that is in agreement with literature. Furthermore, an offset of the martensitic volume change of 0.4 vol% was presented which is attributed to porosity. Data suggests that the amount of porosity affects the measured bulk length change. However, the selectivity between porosity states was not reasonable, as the effect is in the same order as the standard deviation. It is assumed that the pore areas act as free volume for the martensitic transformation, thus leading to a possible reduction in measured overall volume change of the bulk sample.
- Micro-hardness measurements HV0.1 confirmed an independency of porosity on the microstructural hardness, and also a homogeneous distribution between the batches. For both micro- and macro-hardness, models are proposed.
- In the range of common combinations of carbon and nitrogen, a hardness contribution of nitrogen could not be identified. In context of both solved carbon and nitrogen, the resulting hardness in martensite seems exclusively dependent on carbon.

Data availability

The raw/processed data required to reproduce these findings cannot be shared at this time as the data also forms part of an ongoing study.

Conflicts of interest

The authors declare no conflicts of interest.

Acknowledgments

This research was supported by the AiF (grant number 19887 N) within the IGF program from the Federal Ministry of Economic Affairs and Energy (BMWi). The authors also want to thank Höganäs AB for the provision of the material as well IWT Bremen for the heat treatment of the dilatometric samples. Special thanks go to M.Sc. Powdermaker for the analysis of the retained austenite and the IAM-AWP (Chemical Analysis Unit) for the elemental analysis of the decarburized samples. We acknowledge support by the KIT-Publication Fund of the Karlsruhe Institute of Technology.

REFERENCES

[1] Skoglund P, Litstrom O, Flodin A. Improvement of powder metallurgy gears for engines and transmissions; 2013.
[2] Ramakrishnan P. Automotive applications of powder metallurgy. In: Chang ITH, Zhao Y, editors. Advances in powder metallurgy. Woodhead publishing series in metals and surface engineering. Oxford: Woodhead Publishing; 2013. p. 493–519.
[3] Danninger H, Gierl C. Powder metallurgy steels for highly loaded precision parts. Int J Mater Prod Technol 2007;28(3/4):338.
[4] Danninger H, Dlapka M. Heat treatment of sintered steels – what is different? HTM J Heat Treat Mater 2018;73(3):117–30.

[5] Muddle BC, Nie JF. Martensite. In: Buschow KHJ, editor. Encyclopedia of materials. Amsterdam: Elsevier; 2001. p. 5189–93.
[6] Moyer JM, Ansell GS. The volume expansion accompanying the martensite transformation in iron-carbon alloys. Metall Trans A 1975;6(9):1785.
[7] Bose BN, Hawkes MF. Kinetics of the eutectoid transformation in alloys of iron and nitrogen. JOM 1950;2(2):307–16.
[8] van Bohemen S, Sietsma J. Martensite formation in partially and fully austenitic plain carbon steels. Metall Mater Trans A 2009;40(5):1059–68.
[9] Lee S-J, van Tyne CJ. A kinetics model for martensite transformation in plain carbon and low-alloyed steels. Metall Mater Trans A 2012;43(2):422–7.
[10] Guimarães JRC, Rios PR. Quantitative interpretation of martensite microstructure. Mater Res 2011;14(1):97–101.
[11] Sourmail T, Garcia-Mateo C. A model for predicting the M_s temperatures of steels. Comput Mater Sci 2005;34(2): 213–8.
[12] Ishida K. Calculation of the effect of alloying elements on the M_s temperature in steels. J Alloys Compd 1995;220(1):126–31.
[13] Capdevila C, Caballero FG, de Andrés CG. Determination of M_s temperature in steels: A Bayesian neural network model. ISIJ Int 2002;42(8):894–902.
[14] Peet M. Prediction of martensite start temperature. Mater Sci Technol 2015;31(11):1370–5.
[15] Koistinen DP, Marburger RE. A general equation prescribing the extent of the austenite-martensite transformation in pure iron-carbon alloys and plain carbon steels. Acta Metall 1959;7(1):59–60.
[16] Badinier G, Sinclair CW, Allain S, Danoix F, Gouné M. The mechanisms of transformation and mechanical behavior of ferrous martensite. In: Hashmi S, editor. Reference module in materials science and materials engineering. Amsterdam: Elsevier; 2016.
[17] Hollomon JH, Jaffe LD. Ferrous metallurgical design: design principles for fully hardened steel. New York: Wiley; 1947.
[18] Goldschmidt HJ. Advances in X-ray analysis, vol. 5. Plenum Press; 1962. p. 191–212.
[19] Cheng L, Böttger A, de Keijser T, Mittemeijer EJ. Lattice parameters of iron-carbon and iron-nitrogen martensites and austenites. Scr Metall Mater 1990;24(3):509–14.
[20] Tsuchiyama T, Inoue K, Hyodo K, Akama D, Nakada N, Takaki S, et al. Comparison of microstructure and hardness between high-carbon and high-nitrogen martensites. ISIJ Int 2019;59(1):161–8.
[21] Lin L. A method for calculating M_s in multicomponent steels and its application to heat treatment. J Heat Treat 1985;4(2):140–4.
[22] Lombardo S, Steinbacher M. Carbozahn: Carbonitrieren von verzahnten Getriebebauteilen; Abschlussbericht; Forschungsvorhaben Nr. 513 I; 2011.
[23] Nusskern P, Hoffmeister J, Schulze V. Austenite-bainite transformation kinetic model for the powder-metallurgical steel Astaloy 85 Mo. In: Chandra T, Ionescu M, Mantovani D, editors. THERMEC 2011, Materials Science Forum (Pfaffikon). Trans Tech Publications Inc.; 2012. p. 1485–90.
[24] Grevnov LM. Heat treatment of sintered porous steels. Powder Metall Met Ceram 1998;37(11):583–92.
[25] Warke VS, Sisson RD, Makhlouf MM. The effect of porosity on the austenite to bainite transformation in powder metallurgy steels. J Mater Res 2009;24(10):3213–9.
[26] Warke VS, Sisson RD, Makhlouf MM. A model for converting dilatometric strain measurements to the fraction of phase formed during the transformation of austenite to martensite in powder metallurgy steels. Metall Mater Trans A 2009;40(3):569–72.
[27] Dlapka M, Danninger H, Gierl C, Lindqvist B. Defining the pores in PM components. Met Powder Rep 2010;65(2):30–3.
[28] Dlapka M, Danninger H, Gierl C, Lindqvist B. Defining the pores in PM components. Met Powder Rep 2010;65(2):30–3.
[29] Kaiser D, de Graaff B, Dietrich S, Schulze V. A novel procedure to account for high temperature gradients in an induction dilatometer sample during rapid heating. Thermochim Acta 2016;646:8–15.
[30] Damon J, Mühl F, Dietrich S, Schulze V. A comparative study of kinetic models regarding bainitic transformation behavior in carburized case hardening steel 20MnCr5. Metall Mater Trans A 2019;50(1):104–17.
[31] Orlich J, Rose A, Wiest P, editors. Atlas zur Wärmebehandlung der Stähle. Düsseldorf: Verl. Stahleisen; 1973.
[32] Miokovic T, Schwarzer J, Schulze V, Vöhringer O, Löhe D. Description of short time phase transformations during the heating of steels based on high-rate experimental data. In: Denis S, editor. Proceedings of the 2nd International Conference on Thermal Process Modelling and Computer Simulation, Nancy, France, March 31–April 2, 2003. 2004. p. 591.
[33] Walton KS, Snurr RQ. Applicability of the BET method for determining surface areas of microporous metal-organic frameworks. J Am Chem Soc 2007;129(27):8552–6.
[34] Garcia de Andres C, Bartolome MJ, Capdevila C, Martin DN, Caballero F, Lopez V. Metallographic techniques for the determination of the austenite grain size in medium-carbon microalloyed steels. Mater Charact 2001;46(5):389–98.
[35] Garcia de Andres C, Caballero F, Capdevila C, San Martin D. Revealing austenite grain boundaries by thermal etching: advantages and disadvantages. Mater Charact 2002;49(2):121–7.
[36] DIN EN ISO 6507-1:2018-07. Metallische Werkstoffe_- Härteprüfung nach Vickers_- Teil_1: Prüfverfahren (ISO_6507-1:2018); Deutsche Fassung EN_ISO_6507-1:2018; 2018.
[37] ASTM International. E975-13: practice for X-ray determination of retained austenite in steel with near random crystallographic orientation; 2013.
[38] Houdremont E, Krisement O. Betrachtung über die Unterkühlung von Umwandlungsvorgängen als Grundlage für die Martensitumwandlung. Arch Eisenhüttenwes 1953;24(1-2):53–68.
[39] Bramfitt B. Structure/property relationships in irons and steels. In: Davis JR, editor. Metals handbook desk edition, vol. 21. ASM International; 1998. p. 153–73.
[40] Wang J, van der Wolk PJ, van der Zwaag S. Determination of martensite start temperature in engineering steels: part I. Empirical relations describing the effect of steel chemistry. Mater Trans JIM 2000;41(7):761–8.
[41] van Bohemen SMC. Bainite and martensite start temperature calculated with exponential carbon dependence. Mater Sci Technol 2012;28(4):487–95.
[42] Prenosil B. Eigenschaften von durch Diffusion des Kohlenstoffs und Stickstoffs im Austenit entstehenden carbonitrierten Schichten. 2, Die Martensitumwandlung des Fe-CN-Austenits. Härt Tech Mitt 1966;21(2).
[43] Tsyganova MS, Ivashko AG, Tsyganova AI. Prediction of austenite decomposition kinetics in powder steel depending on porosity. IOP Conf Ser: Earth Environ Sci 2018;194(4):042023.
[44] Yang H-S, Bhadeshia HKDH. Uncertainties in dilatometric determination of martensite start temperature. Mater Sci Technol 2007;23(5):556–60.
[45] King HW, Glover SG. A resistometric study of the first stage of tempering in plain carbon steels. J Iron Steel Inst 1959;193:123.

[46] Roberts CS. Effect of carbon on the volume fractions and lattice parameters of retained austenite and martensite. Trans AIME 1953;197(2):203–4.
[47] Marder AR. The morphology of martensite in iron-carbon alloys. Trans ASM 1967;60:651–60.
[48] Ouda K, Danninger H, Gierl-Mayer C. Magnetic measurement of retained austenite in sintered steels – benefits and limitations. Powder Metall 2018;61(5):358–68.
[49] Krauss G, Marder AR. The morphology of martensite in iron alloys. Metall Trans 1971;2(9):2343.
[50] Chiba M, Miyamoto G, Furuhara T. Microstructure of pure iron treated by nitriding and quenching process. J Jpn Inst Met 2012;76(4):256–64.
[51] ASTM Standard. D4780-12: test method for determination of low surface area of catalysts and catalyst carriers by multipoint krypton adsorption; 2017.